Calculation of the conductance of a finite atomic line of sulfur vacancies created on a molybdenum disulfide surface

Kian Soon Yong,[1] Diana M. Otalvaro,[2] Ivan Duchemin,[3] Mark Saeys,[2,4,*] and Christian Joachim[3,4,†]
[1]*Institute of High Performance Computing, Singapore Science Park II, Singapore 117528, Singapore*
[2]*Department of Chemical and Biomolecular Engineering, National University of Singapore, 4 Engineering Drive 4, Singapore 117576, Singapore*
[3]*CEMES, CNRS, 29 rue J. Marvig, 31055 Toulouse Cedex, France*
[4]*Institute of Materials Research and Engineering, 3 Research Link, Singapore 117602, Singapore*
(Received 21 January 2008; revised manuscript received 18 March 2008; published 22 May 2008)

Using the elastic-scattering quantum chemistry technique, it is shown that a surface atomic wire fabricated by extracting a line of S surface atoms from the planar MoS_2 lamellar substrate creates enough electronic states in the MoS_2 surface band gap for this wire to have a large conductance. The nature of the surface electronic states introduced by the S vacancies is investigated for increasing numbers of vacancies for a wire length of up to 10 nm. When contacted by the two Au nanoelectrodes, the wire creates surface pseudoballistic channels and the wire conductance does not decrease with length. The effects of the nanoelectrode-wire distance and of the lateral electrode-wire overlap on the conductance of the wire are also discussed. It is found that the conductance of the junction can be increased threefold by increasing the lateral overlap.

DOI: 10.1103/PhysRevB.77.205429 PACS number(s): 73.63.−b, 71.15.Dx, 85.35.−p

I. INTRODUCTION

Current trends in the miniaturization of electronic devices have generated much interest in fabricating and understanding the properties of atomic-scale structures that can act as wires, switches, transistors, or storage devices.[1–3] Recently, the possibility of manipulating and visualizing single atoms and molecules with atomic precision by using scanning tunneling microscopy (STM) has facilitated the fabrication and study of such structures.[4,5] Besides moving and relocating individual adsorbates on a surface,[6,7] STM can also be used to selectively remove atoms one at a time to create artificial patterns such as atomic lines.[8–12] Fabricated on the surface of a solid substrate, such one-dimensional structures exhibit potential to be used as atomic wires. Small metal islands deposited on such a surface will act as electrodes to contact exactly one atomic wire.[13] The combination of these techniques allows the precise alignment of atomic wires and creates the possibility to experimentally characterize the electrical properties of the wires through the terminal electrodes. In contrast, molecular wires that are made of individual molecules or oligomers[14] are difficult to be reproducibly aligned on a surface with atomic precision that is essential for the wires to be useful in circuit fabrication. Electrical measurements of molecular wires by using crossed-wire junctions, break junctions, and conducting atomic force microscopy are difficult to control, and reliable and reproducible results are challenging to generate.[15]

The creation of atomic lines by extracting atoms from a substrate has been demonstrated on a H-terminated Si(100)-2×1 surface.[4,10–12] Using STM, H atoms can be selectively removed from the Si surface to form an atomic wire comprising of the dangling bonds (DBs) from the exposed Si atoms. As determined by scanning tunneling spectroscopy, such a wire of DBs exhibits a transverse finite density of states near the Fermi energy. In contrast, the H-terminated Si surface shows a wide semiconducting band gap.[10,11] This observation agrees with the first principles theoretical studies by Watanabe *et al.*. These authors also report how the electronic properties of the DB wire depend on the geometry of the wire.[16,17] In a theoretical study by Doumergue *et al.*, the longitudinal conductance of a DB wire was studied in more detail. Taking into account the Peierls distortion of the DB wire, the current was found to decrease with the length of the wire and an inverse decay length of 0.09 $Å^{-1}$ was calculated.[18]

For the MoS_2 surface, the extraction of individual surface S atoms via voltage pulsing with an STM tip has been demonstrated.[19,20] MoS_2 is also a semiconductor, with six S atoms trigonal prismatically coordinated to each Mo atom.[21] Caulfield and Fisher[22] and Fuhr *et al.*[23] have studied the electronic properties of single S vacancies on MoS_2 and reported that such vacancies introduce localized electronic states inside the MoS_2 band gap. Therefore, an atomic line created by the removal of the surface S atoms by using STM is expected to introduce a finite density of states in the MoS_2 band gap, which is localized on the line of S vacancies, and hence show potential for conduction along the atomic wire at low voltage. In addition, different from the DBs on Si, S vacancies on MoS_2 have been found to be quite thermally stable.[20] Furthermore, the deposition and STM manipulation of small Au islands on the MoS_2 surface have recently been demonstrated.[13] Such metallic nanopads can be manipulated to be in electronic contact with the atomic wire of S vacancies and serve as the nanoelectrodes to contact the wire.

In this paper, the electronic properties of a finite line of S vacancies on a MoS_2 surface are theoretically studied for up to a 10 nm wire length. The influence of the two contacting Au electrodes and of the supporting MoS_2 substrate on the electronic structure of the wire is fully taken into account in the calculations. The conductance of the Au pad–MoS_2-Au pad junction is calculated with and without the line of S vacancies. For the perfect MoS_2 surface, the conductance exponentially decreases with the distance between the two

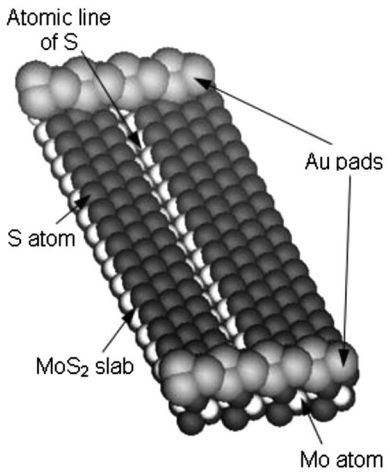

FIG. 1. The atomic model of the junction used to calculate the conductance of a surface atomic wire made of a finite line of S vacancies fabricated on a MoS_2 surface between two Au nanopads. At both ends of the junction, the Au atoms and the MoS_2 substrate below them constitute the first unit cells of the periodic parts of the interconnected semi-infinite wires. Laterally, this structure is repeated by using cyclic boundary conditions.

Au pads. S vacancies are found to introduce electronic states in the MoS_2 surface band gap. Such states near the Fermi level dramatically enhance the conductance of the line. The resulting wire of S vacancies is found to exhibit a conductance that does not decrease with the length of the wire and hence creates pseudoballistic channels for electrons traveling between the two electrodes. To investigate the ways to increase the conductance of the Au pad–wire–Au pad junction, the effect of the Au nanoelectrode-wire distance and the effect of the lateral overlap between the Au nanoelectrodes and the wire on the conductance[24] of the wire were considered.

II. MODELS

The conductance of the Au pad–MoS_2-Au pad junction and that of the line of S vacancies were calculated by using the elastic-scattering quantum chemistry (ESQC) method, which describes using quantum chemistry techniques the scattering of electron waves by a defect embedded in a periodic system.[25,26] The atomic wire of S vacancies was modeled by using the structure shown in Fig. 1, which illustrates the defect as well as the first unit cell of the periodic parts. The wire of S vacancies created on a single layer MoS_2 slab encompasses the defect. The weak interaction with bulk MoS_2 layers underneath was neglected in this study, as had been done by other groups.[22,27] When applying lateral periodic boundary conditions, an eight S atom wide unit cell was used in our study to minimize lateral interactions between neighboring wires. Convergence of the conductance with respect to the unit cell width was confirmed. Wires of 3–31 S vacancies were considered, creating wires of 1.1–10 nm in length, respectively. Surface relaxations introduced by the S vacancies were neglected in this study since calculations by Caulfield and Fisher have shown that the coordinates of the other atoms change very little when a S vacancy is created on MoS_2.[22] The atomic line of S vacancies is contacted by semi-infinite Au nanopads that, together with the underlying MoS_2 substrate, form the periodic system (Fig. 1).

The Bloch states propagating in the plane of the periodic slab consisting of the MoS_2 substrate and the Au nanopads define the incoming and scattered electronic Bloch states that are used to calculate the transmission amplitudes and the junction conductance. Using ESQC, the valence electronic structures of the wire, of the MoS_2 substrate, and of the Au pads are taken into account using a minimal linear combination of atomic orbital representation. Effects of the finite size of the wire, of the contact resistance between the wire and the Au pads, and of the coupling with the MoS_2 substrate are considered fully in our theoretical model. In our largest junction, the two Au nanopads define a 10 nm junction and the defect region with the atomic line of S vacancies comprises 744 atoms and 4216 atomic orbitals, including the full valence description of the S and Mo atoms. Because of the size of the system, *ab initio* calculations become impractical and the extended Hückel molecular orbital (EHMO) model[28] was used in ESQC to construct the electronic Hamiltonian. The standard Hückel parameters[29] were used in the calculations. Within such a model, electron-phonon interactions, inelastic scattering, and finite temperature effects are neglected.

To analyze the nature of the states introduced by the S vacancies, their interactions, and also to elucidate the dispersive characteristics of the bands responsible for the surface conductance of MoS_2 and of the wire of S vacancies, a number of additional calculations were performed using the EHMO model. The band structures and density of states (DOS) of MoS_2 (Fig. 2) and of an infinite line of S vacancies on the surface of a MoS_2 substrate (Fig. 7) were calculated using BICON-CEDIT.[30] The standard EHMO parameters were used in these calculations, thus preserving consistency with the ESQC results. Moreover, to corroborate the EHMO band structures at a higher level of electronic correlation, density functional theory (DFT) calculations were performed for MoS_2 and for an infinite wire of S vacancies by using the Perdew–Burke–Ernzerhof (PBE) functional,[31] plane augmented wave pseudopotentials, and a fine k-point grid as implemented in the Vienna *Ab initio* simulation package (VASP).[32] Furthermore, EHMO calculations on large MoS_2 clusters were employed using GAUSSIAN03[33] to help identify the states introduced by a S vacancy and their interactions. A $Mo_{83}S_{166}$ cluster with D_{3h} symmetry was used to model the MoS_2 slab. The size of the clusters was chosen to ensure that the edge states, intrinsic in any finite cluster approximation, would not contribute to the states of interest. Initially, a single S atom was removed and the molecular orbitals (MOs) of the resulting structure were examined. Sequentially, S atoms adjacent to the vacancy were removed to form a finite line of up to ten S vacancies and the resulting MOs were again investigated.

III. RESULTS

A. Surface MoS_2 nanojunction

Before discussing the results for the atomic wires of S vacancies, the electronic properties of an Au pad–MoS_2-Au

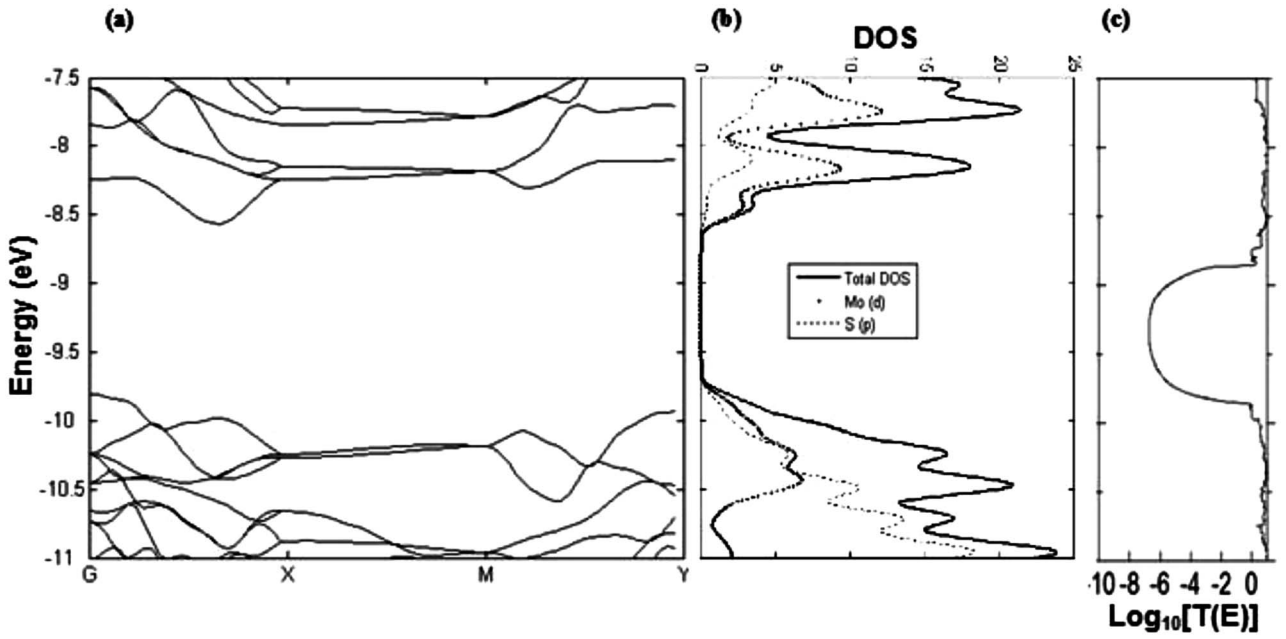

FIG. 2. The electronic characteristics of the MoS_2 surface with (a) the MoS_2 band structure calculated with a $c(2\times2)$ unit cell, (b) the corresponding total density of states projected on the Mo (d) and S (p) orbitals, and (c) the MoS_2 surface electronic $T(E)$ transmission coefficient for a 2.1 nm internanopads distance in the Fig. 1 junction. $T(E)$ is calculated in the direction of the wire, while the total DOS is integrated over the entire Brillouin zone.

pad junction are discussed. Since MoS_2 is a semiconductor with an estimated 1.0 eV electronic surface band gap, the surface tunneling probability between the two Au nano-pads will be very small for electrons in this energy range. The results in this section will serve as a reference when calculating the conductance of a finite line of S vacancies. To interpret the results, the MoS_2 band structure and the corresponding DOS are also shown in Figs. 2(a) and 2(b), respectively. The indirect 1 eV band gap is similar to the previous calculations at the EHMO level[34] and slightly lower than the experimental transverse band gap of 1.3 eV.[35] The EHMO band structure is qualitatively similar to the DFT band structure,[36] although the band gap calculated by the PBE functional is slightly larger at 1.5 eV. The transmission coefficient $T(E)$ for a junction of 2.1 nm between two Au nanopads is displayed in Fig. 2(c). For energies within the MoS_2 conduction and valence bands, the Bloch states in the MoS_2 surface band structure can freely propagate and the junction does not scatter the incoming electrons. However, no states are available in the junction for energies within the MoS_2 band gap and $T(E)$ is significantly reduced for electron waves traveling on the Au pads within this energy range. The parabolic shape of the logarithm (to base ten) of $T(E)$ in the band gap results from the overlap of the broadened states at the top of the MoS_2 valence band and at the bottom of the MoS_2 conduction band in the junction.[37] When the electronic states in the junction couple to the semi-infinite metal electrodes, they broaden to the Lorentzian-type peaks. The width of the peaks and hence the precise shape of the parabola depend on the interfacial coupling between the state and the electrodes. Close correspondence between the MoS_2 band structure and $T(E)$ can be observed, indicating the direct relationship between the energy dependence of the electronic transparency of a junction and its electronic band structure.

The $T(E)$ variation of the junction, as a function of the surface distance between the two Au nanopads, is plotted in Fig. 3, selecting, for example, the minimum of $T(E)$ per wire length. Following this plot, the junction electronic transparency exponentially decreases with its length, which is a characteristic of a tunneling transport regime through a junction.[18,38] At the Fermi level, the variation of $T(E)$ with the junction length can be expressed as[18,39]

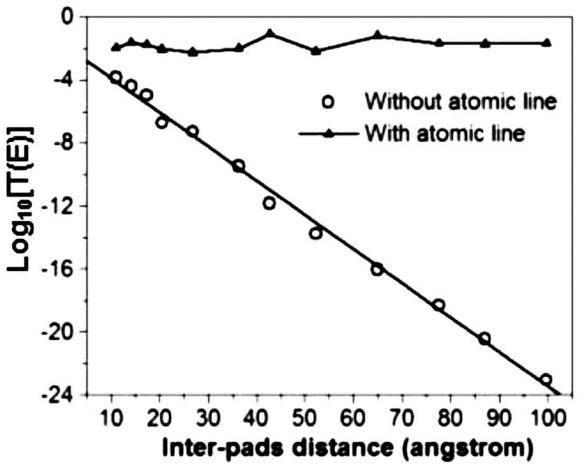

FIG. 3. The variation of the transmission coefficient at the Fermi level as a function of the distance between the two Au nanopads for a surface MoS_2 junction (○) and for an atomic wire of S vacancies fabricated on the MoS_2 surface (▲) whose structure is given in Fig. 1.

$$T(d) = T_0 e^{-\gamma d}, \tag{1}$$

where γ and d describe the inverse decay length and the interpad distance, respectively. The inverse decay length γ is a damping factor that characterizes the intrinsic electronic structure of the junction and depends on the destructive interferences of the electron waves traveling on the MoS_2 surface. An inverse decay length of 0.22 $Å^{-1}$ was calculated for MoS_2. This value is much smaller than for tunneling through vacuum (γ=2.21 $Å^{-1}$) and slightly smaller than the value for a hydrogenated Si(100)-2×1 surface (γ=0.41 $Å^{-1}$), which is consistent with the larger band gap of ~2 eV for the latter.[18]

Theoretical studies have expressed the inverse decay length γ as a function of the gap χ between the highest-occupied molecular orbital (HOMO) and the lowest-unoccupied molecular orbital (LUMO) of the junction, the position of the frontier orbitals, and the effective mass ($m*$) of the electron tunneling between the Au electrodes.[24,40] Specifically,

$$\gamma(E) = \sqrt{\frac{2m^*(E)}{\hbar^2}\frac{(E-E_h)(E_l-E)}{\chi}}, \tag{2}$$

where E_h and E_l are the HOMO and LUMO energies, respectively. For the MoS_2 junction, $\gamma(E_F)$=0.22 $Å^{-1}$ and χ is equal to the MoS_2 band gap of 1.07 eV (Fig. 2). With these values, an effective mass $m^*(E_F)$ of $0.70m_e$ is obtained, where m_e is the rest mass of the electron.

B. Wire of S vacancies on a MoS_2 surface

It had been experimentally shown that S atoms can be selectively removed from a MoS_2 surface via field evaporation by using an STM tip.[19,20] Theoretical studies of the electronic structure of a single S vacancy on MoS_2 indicate that removing a S atom introduces states in the MoS_2 band gap.[22,23] Therefore, it is expected that an atomic wire consisting of a number of neighboring S vacancies would exhibit several electronic states within the band gap. The calculated $T(E)$ for a line of seven S vacancies (2.1 nm) is shown in Fig. 4. At the Fermi level, −9.4 eV, the $T(E)$ of the wire is about 10^{-2} and a factor 10^4 larger than for a surface MoS_2 junction of the same length but with no vacancies. The removal of S atoms introduces a number of states in the surface MoS_2 band gap, as obvious from the sharp peaks in the $T(E)$ spectrum presented in Fig. 4. To help interpret such a spectrum, calculations of the band structure and the corresponding DOS for an infinite periodic S vacancy line were performed.

Each S vacancy formed on a MoS_2 surface creates three dangling bonds, one on each of the Mo atoms, which was coordinated to the extracted S. Accordingly, the transmission spectrum for a MoS_2 junction with a single vacancy shows new peaks in the band gap, resulting from resonant tunneling (not shown). EHMO calculations on a large MoS_2 cluster corroborate such finding by showing three MOs centered on the vacancy (Fig. 5), with energies coinciding with the resonant peaks in the transmission spectrum. Two of the MOs [Figs. 5(a) and 5(b)] are degenerate by symmetry, as identified by the orientation of their nodal planes normal to the surface. For the MO in Fig. 5(a), this nodal plane is oriented along the positive xy axis, and for the MO in Fig. 5(b), it is aligned with the negative xy axis. Because of the degeneracy of these two states, they lead to a single peak in the transmission spectrum. Energetically, the degenerate MOs lie near the Fermi level and significantly contribute to the transmission. A third symmetric MO is found near the top of the MoS_2 valence band and coincides with a peak in the transmission spectrum.

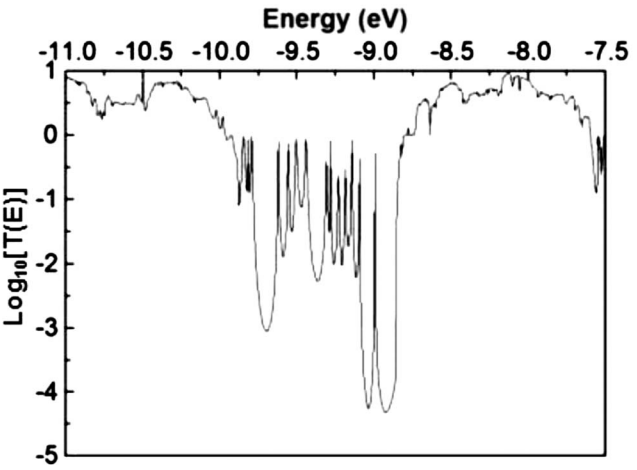

FIG. 4. The ESQC calculated $T(E)$ transmission coefficient spectrum for a wire of seven S vacancies (2.1 nm) fabricated on a MoS_2 surface between two Au nanopads. The 16 resonances can be identified whose attributions are discussed in the text.

Based upon these observations, it is expected that a wire of neighboring S vacancies introduces several electronic states within the band gap, which spread over an energy range around the Fermi level. This is confirmed by the EHMO calculations shown in Fig. 6. Each additional S vacancy gives rise to new states in the gap, and the spacing between the states is indicative of the interaction between adjacent MOs. The MOs originating from the degenerate pair split considerably after each S removal, which is an indication of the relatively strong interaction, while the MOs originating from the symmetric MO split considerably less and remain located near the top of the valence band. Some of the bonding combinations corresponding to the symmetric MO shift below the top of the valence band and are not represented in Fig. 6. Consequently, for an infinite line of S vacancies, three bands emerge in the MoS_2 band gap as can be seen by comparison of the band structures for MoS_2 and the infinite line shown in Figs. 2(a) and 7(a), respectively. To generate the band structure for the infinite line, a rectangular 4×1 unit cell consisting of four MoS_2 primitive unit cells was used. A single S atom was removed per unit cell to create an infinite line of S vacancies. The absence of dispersion for the three new bands in the X-M direction perpendicular to the atomic wire verifies the one-dimensional character of the electronic states localized along the wire of S vacancies. The EHMO band structure and DOS are again qualitatively similar to the DFT-PBE band structure that was calculated for comparison.[36]

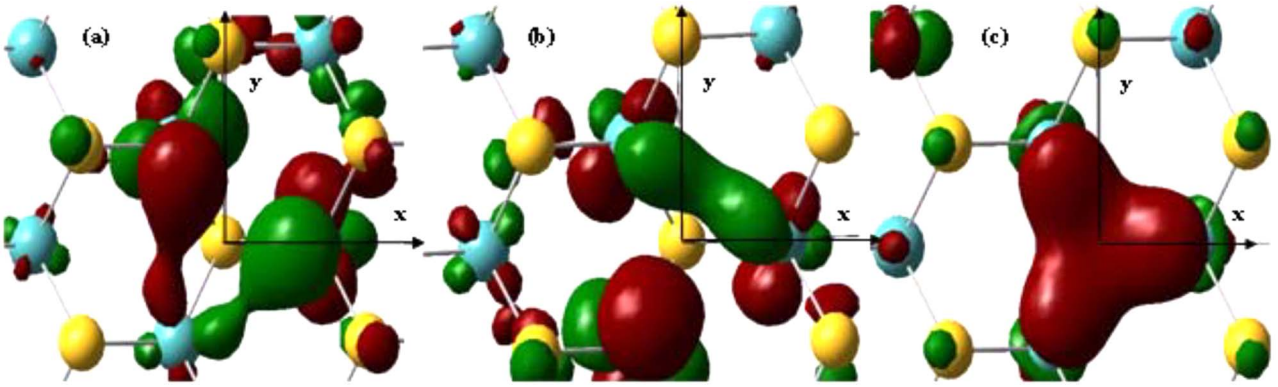

FIG. 5. (Color online) Representation of the molecular orbital changes introduced in the MoS_2 band gap by extracting a S atom, which is located at the origin of the coordinate system. (a) and (b) are the degenerate MO pair at the center of the MoS_2 band gap and (c) is the symmetric MO near the top of the MoS_2 valence band. The different colors correspond to different phases of the wave function for the molecular orbital.

The transmission calculations were repeated for atomic wires of different lengths and comparison of the results shows that each removal of an additional S atom introduces new states in the band gap while the previously introduced states are redistributed in energy. The various states have different strengths and widths, which can be attributed to the difference in coupling of the states with the Au pads. Strong (weak) coupling interactions produce broad (narrow) peaks. Figure 3 shows the variation of the conductance of the atomic wires with length as defined by the distance between the Au pads. The conductance of an atomic wire of S vacancy line does not decrease with length, as in the case of a MoS_2 junction. Hence, the atomic line creates pseudo-ballistic channels for the conduction of electrons between the two Au electrodes. Those are not exactly ballistic because of the finite length of the wire which preserves as presented in Fig. 4 a distribution of resonances and not an exact $T(E)=1$ over the full energy range of high electronic transparency created by this wire. Furthermore, the resonance maxima in $T(E)$ spectra, as presented in Fig. 3, are less than 1 because the electronic contact between the Au electrode and the atomic wire scatters the incoming electron waves. The oscillations of $T(E)$ with the wire length are caused by small shifts in the positions of the resonances with respect to the Fermi level every time the length of the wire increases by one S vacancy.

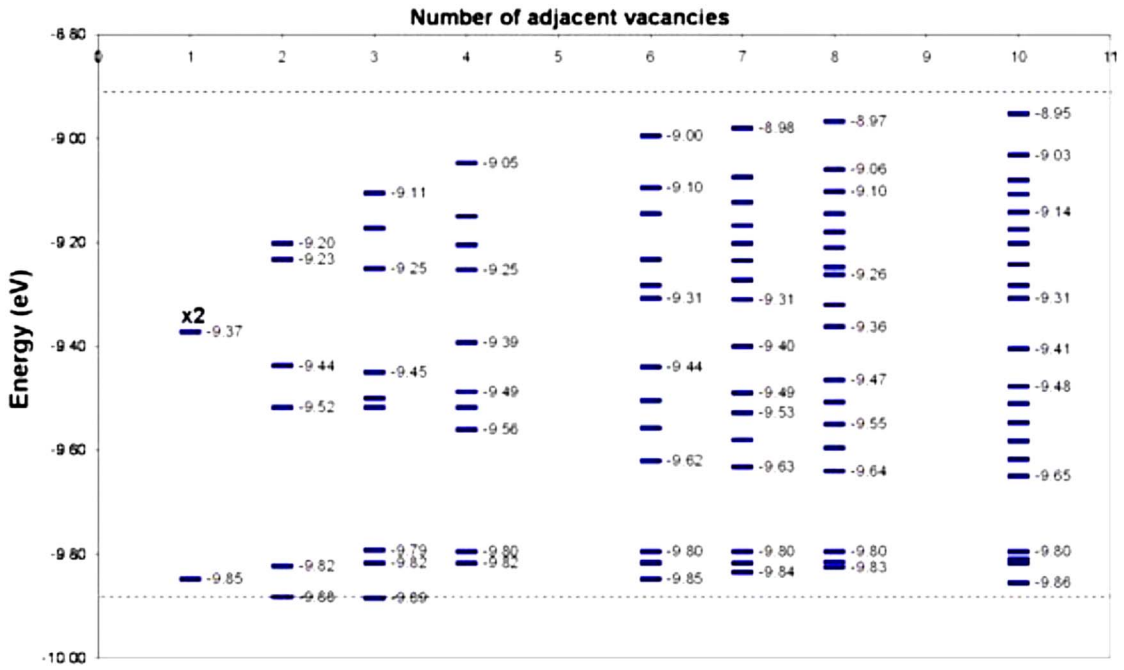

FIG. 6. (Color online) Diagram illustrating the energy distribution of the states introduced in the MoS_2 band gap by the successive extraction of adjacent S atoms. The dashed lines indicate the bottom of the conduction and top of the valence band. Notice the slow process of introducing states, created by S vacancies, in the range between the two bands near the center of the MoS_2 surface band gap. Even for $N=10$, there is still an apparent energy range between −9.41 and −9.31 eV without wire states.

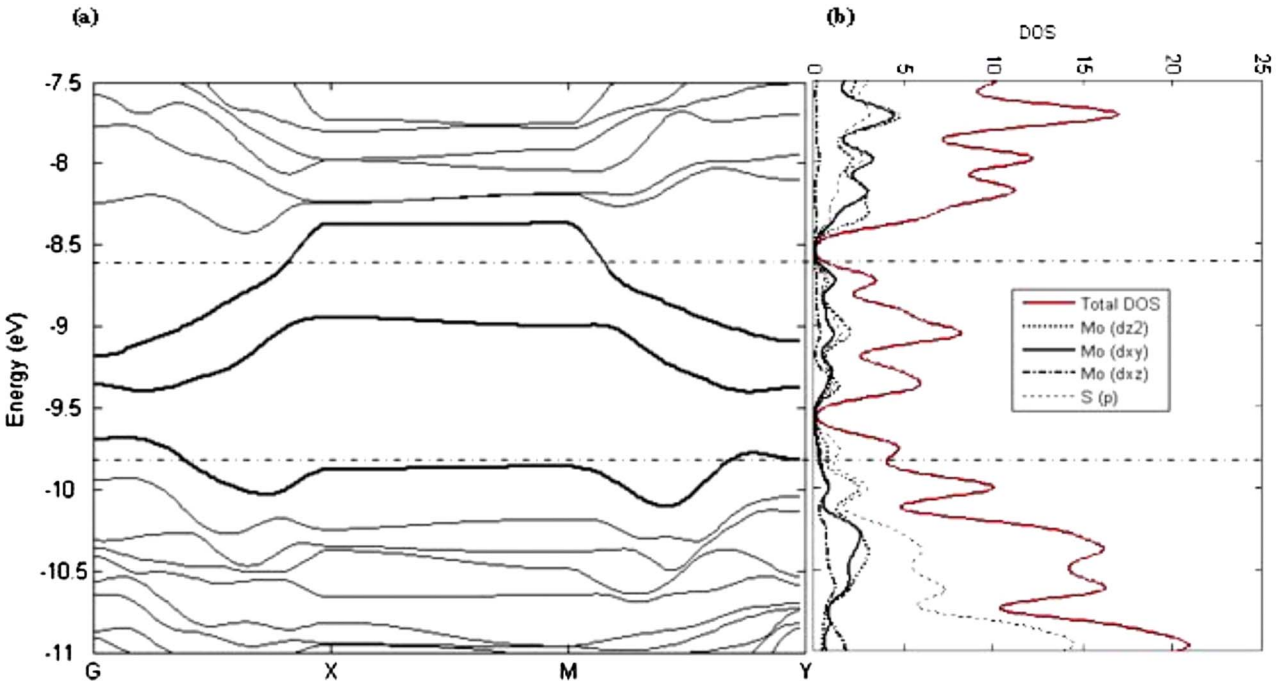

FIG. 7. (Color online) The electronic characteristics of the MoS_2 surface with an atomic line of S vacancies. (a) Band structure for an infinite line of S vacancies, created by removing one S atom per unit cell for a rectangular (4×1) MoS_2 unit cell, and (b) the corresponding total density of states, projected on the Mo d_{z^2}, Mo d_{xy}, d_{xz}, and S p orbitals. For reference, the conduction and valence band edges for the MoS_2 slab are indicated by the dashed lines.

C. Contact conductance G_0

In molecular electronics, good electrical contacts between different circuit elements are critical for reliable transport of current signals.[41] Similarly, in the current Au pad–atomic wire–Au pad junction, the electronic coupling of the atomic wire with the Au electrodes determines the ease of electron flow between the two electrodes through the atomic wire. Such electronic interactions are characterized by G_0, the so-called contact conductance of the atomic wire, which is, in turn, related to G, which is the low voltage conductance of the junction. G can be determined from $T(E)$ at the Fermi level [Eq. (1)] using the Landauer formula,[42]

$$G = \frac{2e^2}{h} T(E_F), \tag{3}$$

which leads to a direct correspondence to Eq. (1) in terms of G and G_0 as given by[24,40]

$$G = G_0 e^{-\gamma d}. \tag{4}$$

To increase the contact conductance G_0 and hence increase the current that can flow through the wire, the effect of the distance h between the Au electrodes and the MoS_2 surface and of the lateral overlap of the Au electrode with the wire of S vacancies on the conductance of the junction were explored.

To investigate the effect of the electrode height h on G_0, plots of $T(E)$, similar to that shown in Fig. 4, were obtained for various lengths of the atomic wire. The transmission coefficients $T(E_F)$ at the Fermi level were collected for various heights h and for various wire lengths. For each height h, the average $T(E_F)$ for atomic wires of different lengths was calculated. The contact conductance G_0 as a function of the electrode height h is shown in Fig. 8(a). The contact conductance G_0 reaches a maximum when Au electrode-surface distance is about 2.4 Å. When the Au pad is further away from the MoS_2 surface, the decreased overlap between the Au orbitals and the states on the wire reduces the coupling between the electrodes and the wire and reduces G_0. When the Au pad is too close to the MoS_2 surface, the coupling between the electrode and the wire is very large. In this case, the electronic structure of the Au nanopads nearby the wire is also modified. This new electronic disorder creates a large reflection of the incoming electron waves and the contact conductance decreases again. Both effects can be well reproduced using a tight-binding model of an atomic wire that is electronically coupled to two electrodes. This tight-binding model, as shown in Appendix [Fig. 9], demonstrates that an optimal height h (or orbital overlap) leads to a maximal contact conductance G_0. In addition, our calculations confirmed that the inverse decay length γ for the Au electrode–MoS_2–Au electrode junction without the atomic wire does not change for different heights h. This shows that changes in the interaction between the junction and the Au pads only affect G_0 but not γ, which is consistent with the data for the conductance of oligomer wires.[43]

To investigate methods to increase the conductance of the atomic wire junction, the effect of sliding the Au electrodes over the wire of S vacancies, thereby increasing the lateral overlap between the Au electrodes and the atomic wire, on the conductance is also investigated. In the calculations, the distance between the electrodes was kept constant at 3.3 nm,

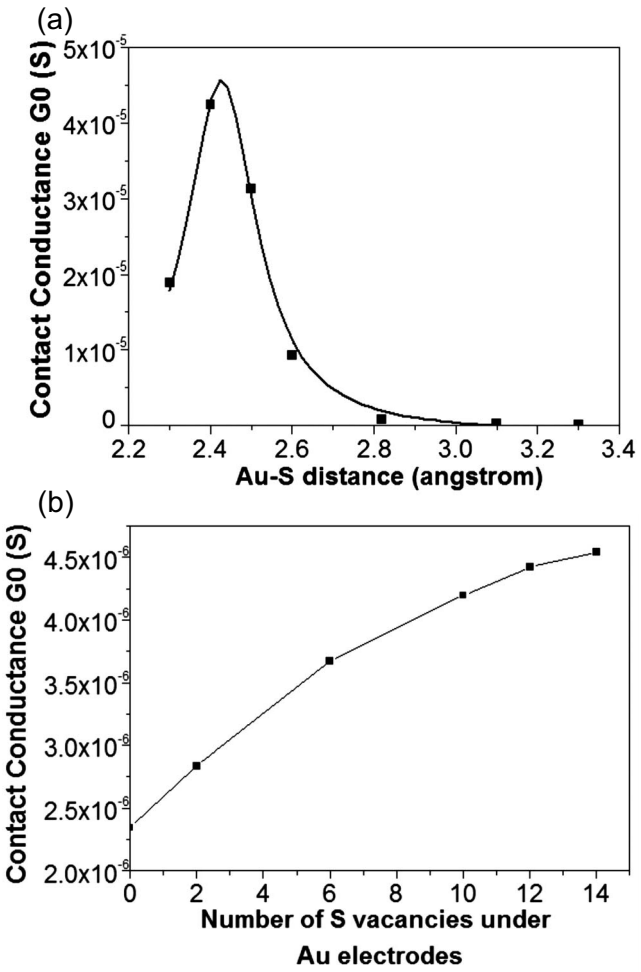

FIG. 8. The contact conductance G_0 for an Au pad–atomic wire–Au pad junction as a function of (a) the height of the Au pad above the MoS_2 surface and (b) the overlap of the Au nanopads over the atomic wire for a fixed interelectrode distance of 3.3 nm.

but the length of the wire of S vacancies was gradually increased from 3.3 to 7.8 nm. In this way, the overlap between the electrodes and the wire was increased from 0 to 7 vacancies per electrode, keeping the length of the junction constant. The contact conductance G_0 as a function of the number of S vacancies under the Au electrodes is plotted in Fig. 8(b). The conductance of the junction can be increased by a factor 3 by sliding the electrodes over the wire, but saturates for an overlap of seven to eight vacancies per electrode.

IV. DISCUSSION

In the following and to investigate the states responsible for the pseudoballistic channel of the surface atomic wire, the nature and origin of the three MOs introduced by removing a S atom are now discussed further. The symmetric MO [Fig. 5(c)] is almost uniquely composed of π bonded Mo d_{z^2} atomic orbitals and is located near the top of the valence band. The degenerate pair is mainly composed of Mo d_{xz} and d_{yz} orbitals and lies at the center of the MoS_2 band gap. The three molecular orbitals do not show significant contributions

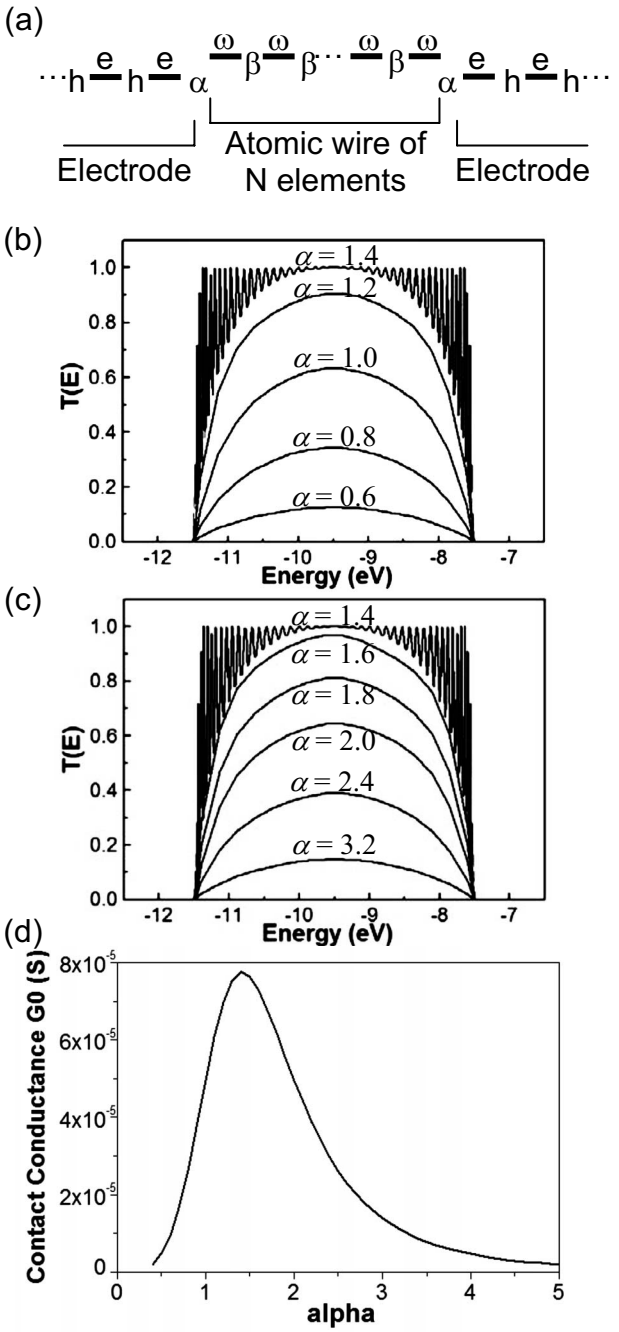

FIG. 9. (a) Tight-binding model of the electrode-atomic wire-electrode system used to study the effect of the wire-electrode coupling α on $T(E)$ for α in the range (b) from 0.6 to 1.4 and (c) from 1.4 to 3.2 (b). Other parameters are β=1.0, h=2, $e=\omega=-9.5$, and N=50. Variation of G_0 as a function of α is shown in (d). For clarity, the wire resonances have been kept only for α=1.4.

from the neighboring S atoms, as confirmed by the linear combination of atomic orbital decomposition of the molecular orbitals. Looking more carefully at the formation of these new states, it was possible to track their origin. In the original MoS_2, the S(p) and Mo(d) orbitals form bonding and antibonding states located in the valence and conduction bands, respectively. When the S atom is gradually removed to create a vacancy, molecular orbital calculations indicate

that the originally antibonding Mo(d)-S(p) state stabilizes and localizes in the gap and transforms to the Mo(d) state observed for the S vacancy, while the bonding state destabilizes and becomes localized on the removed S atom.

Moving gradually toward the infinite line, it is helpful to investigate the interactions observed for two to ten neighboring S vacancies. Each additional S vacancy introduces three new states, and the orbitals on neighboring sites interact to form bonding and antibonding combinations. Examination of the symmetry and spatial characteristics of the MOs resulting from the degenerate pair indicates that they mix, that is, that the different symmetries of the MO pair evident in Figs. 5(a) and 5(b) are not preserved during the formation of the vacancy line. Since the symmetric MO is more localized on the vacancy, the states arising from it less strongly interact. Thus, Fig. 6 evinces that the gradual formation of the line of S vacancies leads to the formation of three bands in the gap. By projecting the DOS onto the different orbitals, it is possible to characterize their contributions. This procedure reveals that the two bands originating from the degenerate states consist of a mixture of all Mo d orbitals. Indeed from the MO diagram in Fig. 6, it can be concluded that there is no one-to-one correspondence between a band and a degenerate state, but rather that both degenerate states are mixed to a different extend for different points in the Brillouin zone. Further evidence for the mixing of the states can be obtained from Fig. 7. The two bands near the center of the MoS_2 gap exhibit a $\cos(kx)$-type energy dispersion along the wire between G and X and between M and Y. The corresponding DOS indeed shows two corresponding peaks, and the central peak shows a shoulder resulting from the overlap between the top and bottom peaks of the two bands [Fig. 7(b)]. For the wire of ten S vacancies, the spread in the energy spectrum of the states originating from the degenerate pair span nearly 0.7 eV, very similar to the dispersion of the bands for the infinite wire.

Moreover, the projected DOS and the band structure of the wire of S vacancies reveal a strong hybridization of the Mo d orbitals on the vacancies. This hybridization accounts for the broad peaks in the band gap. The dispersion of the two bands originating from the degenerate pair arises from π-type interactions between Mo d orbitals in the plane of the wire, while interactions between Mo d_{z^2} orbitals are responsible for the smaller dispersion of the band originating from the symmetric MO.

V. CONCLUSIONS

It has been theoretically demonstrated that a finite atomic line of S vacancies created on a planar MoS_2 substrate can function as a pseudoballistic wire for electron transport. This wire can be formed by extracting S atoms from the MoS_2 surface. Removing surface S atoms introduces electronic states within the surface MoS_2 electronic band gap. Each S vacancy introduces a symmetric molecular orbital of mainly Mo d_{z^2} character near the top of the valence band and a degenerate pair of molecular orbitals of mainly Mo d_{xz} and d_{yz} character near the center of the band gap. Mixing of the degenerate orbitals on neighboring vacancies causes the gradual formation of two overlapping energy bands near the Fermi level, which create pseudoballistic electron transport channels. The conductance of the wire is independent of its length, but the overall channel transparency is not reaching unity. The conductance of an Au electrode–atomic wire–Au electrode junction can be enhanced by optimizing the Au electrode-wire distance and by increasing the lateral Au electrode-wire overlap by sliding the electrode over the wire.

ACKNOWLEDGMENTS

The authors wish to thank the A*STAR VIP "Atom Technology" project and NUS for financial support and N. Chandrasekhar for useful discussion.

APPENDIX: TIGHT-BINDING MODEL

To illustrate the influence of the electronic coupling between an atomic wire and its electrodes on the $T(E)$ of the wire, a tight-binding model was constructed [Fig. 9(a)]. The atomic wire has an intrawire coupling β and is coupled to the electrodes by α. The hopping integral within the electrode is h, while ω and e are the energy levels for, respectively, the wire and the electrodes. The $T(E)$ for this system is calculated using standard formula.[38] It can be shown that the conductance depends on α, which is the electronic coupling between the wire and the electrodes. Figures 9(b) and 9(c) show the variation of the $T(E)$ as a function of the wire-electrode coupling α. Under such situations [Eqs. (3) and (4)], G_0 is proportional to $T(E_F)$ and reaches an optimal value of 1 when $\alpha=1.4$ for $h=2.0$, $\beta=1.0$ eV, and $e=\omega$. The variation of G_0 as a function of α is plotted in Fig. 9(d) and helps in the understanding of the result in Fig. 8(a).

*chesm@nus.edu.sg
†joachim@cemes.fr

[1] Y. Wada, M. Tsukada, M. Fujihira, K. Matsushige, T. Ogawa, M. Haga, and S. Tanaka, Jpn. J. Appl. Phys., Part 1 **39**, 3835 (2000).
[2] C. Joachim, J. K. Gimzewski, and A. Aviram, Nature (London) **408**, 541 (2000).
[3] R. L. Carroll and C. B. Gorman, Angew. Chem., Int. Ed. **41**, 4378 (2002).
[4] T.-C. Shen, C. Wang, G. C. Abeln, J. R. Tucker, J. W. Lyding, Ph. Avouris, and R. E. Walkup, Science **268**, 1590 (1995).
[5] K. Sattler, Jpn. J. Appl. Phys., Part 1 **42**, 4825 (2003).
[6] D. M. Eigler and E. K. Schweizer, Nature (London) **344**, 524 (1990).
[7] T. A. Jung, R. R. Schlittler, J. K. Gimzewski, H. Tang, and C. Joachim, Science **271**, 181 (1996).
[8] J. W. Lyding, T.-C. Shen, J. S. Hubacek, J. R. Tucker, and G. C. Abeln, Appl. Phys. Lett. **64**, 2010 (1994).

[9] J. W. Lyding, Proc. IEEE **85**, 589 (1997).
[10] T. Hitosugi, T. Hashizume, S. Heike, S. Watanabe, Y. Wada, T. Hasegawa, and K. Kitazawa, Jpn. J. Appl. Phys., Part 2 **36**, L361 (1997).
[11] T. Hitosugi, T. Hashizume, S. Heike, H. Kajiyama, Y. Wada, S. Watanabe, T. Hasegawa, and K. Kitazawa, Appl. Surf. Sci. **130-132**, 340 (1998).
[12] L. Soukiassian, A. J. Mayne, M. Carbone, and G. Dujardin, Surf. Sci. **528**, 121 (2003).
[13] J. Yang, J. Deng, N. Chandrasekhar, and C. Joachim, J. Vac. Sci. Technol. B **25**, 1694 (2007).
[14] D. K. James and J. M. Tour, Top. Curr. Chem. **257**, 33 (2005).
[15] D. K. James and J. M. Tour, Chem. Mater. **16**, 4423 (2004).
[16] S. Watanabe, Y. A. Ono, T. Hashizume, Y. Wada, J. Yamauchi, and M. Tsukada, Phys. Rev. B **52**, 10768 (1995).
[17] S. Watanabe, Y. A. Ono, T. Hashizume, and Y. Wada, Phys. Rev. B **54**, R17308 (1996).
[18] P. Doumergue, L. Pizzagalli, C. Joachim, A. Altibelli, and A. Baratoff, Phys. Rev. B **59**, 15910 (1999).
[19] S. Hosoki, S. Hosaka, and T. Hasegawa, Appl. Surf. Sci. **60-61**, 643 (1992).
[20] S. Hosaka, S. Hosoki, T. Hasegawa, H. Koyanagi, T. Shintani, and M. Miyamoto, J. Vac. Sci. Technol. B **13**, 2813 (1995).
[21] R. G. Dickinson and L. Pauling, J. Am. Chem. Soc. **45**, 1466 (1923).
[22] J. C. Caulfield and A. F. Fisher, J. Phys.: Condens. Matter **9**, 3671 (1997).
[23] J. D. Fuhr, A. Saúl, and J. O. Sofo, Phys. Rev. Lett. **92**, 026802 (2004).
[24] S. Stojkovic, C. Joachim, L. Grill, and F. Moresco, Chem. Phys. Lett. **408**, 134 (2005).
[25] P. Sautet and C. Joachim, Chem. Phys. Lett. **153**, 511 (1988).
[26] P. Sautet and C. Joachim, Chem. Phys. Lett. **185**, 23 (1991).
[27] R. Rytz and G. Calzaferri, J. Phys. Chem. B **101**, 5664 (1997).
[28] R. Hoffmann, J. Chem. Phys. **39**, 1397 (1963).
[29] R. H. Summerville and R. Hoffmann, J. Am. Chem. Soc. **98**, 7240 (1976).
[30] M. Brandle, R. Ruedi, and G. Calziferri, BICON-CEDIT, University of Berne, 1997.
[31] J. P. Perdew, K. Burke, and M. Ernzerhof, Phys. Rev. Lett. **77**, 3865 (1996).
[32] G. Kresse and J. Hafner, Phys. Rev. B **47**, 558 (1993).
[33] M. J. Frisch, G. W. Trucks, H. B. Schlegel, G. E. Scuseria, M. A. Robb, J. R. Cheeseman, J. A. Montgomery, Jr., T. Vreven, K. N. Kudin, J. C. Burant, J. M. Millam, S. S. Iyengar, J. Tomasi, V. Barone, B. Mennucci, M. Cossi, G. Scalmani, N. Rega, G. A. Petersson, H. Nakatsuji, M. Hada, M. Ehara, K. Toyota, R. Fukuda, J. Hasegawa, M. Ishida, T. Nakajima, Y. Honda, O. Kitao, H. Nakai, M. Klene, X. Li, J. E. Knox, H. P. Hratchian, J. B. Cross, V. Bakken, C. Adamo, J. Jaramillo, R. Gomperts, R. E. Stratmann, O. Yazyev, A. J. Austin, R. Cammi, C. Pomelli, J. W. Ochterski, P. Y. Ayala, K. Morokuma, G. A. Voth, P. Salvador, J. J. Dannenberg, V. G. Zakrzewski, S. Dapprich, A. D. Daniels, M. C. Strain, O. Farkas, D. K. Malick, A. D. Rabuck, K. Raghavachari, J. B. Foresman, J. V. Ortiz, Q. Cui, A. G. Baboul, S. Clifford, J. Cioslowski, B. B. Stefanov, G. Liu, A. Liashenko, P. Piskorz, I. Komaromi, R. L. Martin, D. J. Fox, T. Keith, M. A. Al-Laham, C. Y. Peng, A. Nanayakkara, M. Challacombe, P. M. W. Gill, B. Johnson, W. Chen, M. W. Wong, C. Gonzalez, and J. A. Pople, GAUSSIAN03 Revision C.02, Gaussian, Inc., Wallingford, CT, 2004.
[34] L. F. Matteiss, Phys. Rev. Lett. **30**, 784 (1973); Phys. Rev. B **8**, 3719 (1973).
[35] T. Böker, R. Severin, A. Müller, C. Janowitz, R. Manzke, D. Voß, P. Krüger, A. Mazur, and J. Pollmann, Phys. Rev. B **64**, 235305 (2001).
[36] See EPAPS Document No. E-PRBMDO-77-084816 for the DFT calculated band structure of MoS_2 and of an infinite line of S vacancies created on a MoS_2 surface. For more information on EPAPS, See http://www.aip.org/pubservs/epaps.html
[37] Y. Xue and M. A. Ratner, Int. J. Quantum Chem. **102**, 911 (2005).
[38] M. Magoga and C. Joachim, in *Atomic and Molecular Wires*, edited by C. Joachim and S. Roth (Kluwer Academic, Boston, 1997) p. 219.
[39] M. Magoga and C. Joachim, Phys. Rev. B **57**, 1820 (1998).
[40] C. Joachim and M. Magoga, Chem. Phys. **281**, 347 (2002).
[41] K. W. Hipps, Science **294**, 536 (2001).
[42] M. Büttiker, Y. Imry, R. Landauer, and S. Pinhas, Phys. Rev. B **31**, 6207 (1985).
[43] M. Magoga and C. Joachim, Phys. Rev. B **56**, 4722 (1997).